Phase stability of (Al$_x$Ga$_{1-x}$)$_2$O$_3$ polymorphs: A first-principles study

Sai Mu ⬤ and Chris G. Van de Walle ⬤[*]

Materials Department, University of California, Santa Barbara, California 93106, USA

Monoclinic Ga$_2$O$_3$ and (Al$_x$Ga$_{1-x}$)$_2$O$_3$ alloys are wide-band-gap semiconductors with promising applications in power electronics. Although the physical properties of monoclinic Ga$_2$O$_3$ (β phase) have been extensively explored, information is lacking about other phases (α, γ, κ) of Ga$_2$O$_3$ and related alloys. Here we use density functional theory to assess the phase stability of different polymorphs of Ga$_2$O$_3$ and (Al$_x$Ga$_{1-x}$)$_2$O$_3$ alloys at both zero and finite temperatures. Due to the preference of Al for the octahedral site, the γ and κ phases of (Al$_x$Ga$_{1-x}$)$_2$O$_3$ exhibit a minimum enthalpy of formation at 62.5% and 50% Al concentrations, respectively. Relative to the other phases, the enthalpy of formation of the γ phase is the highest over the entire range of alloy compositions. We examined the effect of strain arising from pseudomorphic growth of (010)-oriented (Al$_x$Ga$_{1-x}$)$_2$O$_3$ films on β-Ga$_2$O$_3$ substrates and found that the alloys become less stable. At finite temperature we found that the lattice vibrations tend to stabilize the κ phase and destabilize the α and γ phases, referenced to the monoclinic phase. This can be attributed to the greater phonon density of states of the κ phase at low frequencies. A unique configurational entropy that is present in the γ phase due to the cation vacancy disorder plays a substantial contribution in stabilizing the γ phase at finite temperature, particularly at 50% Al concentration. Our study provides a comprehensive overview of stability of different phases of (Al$_x$Ga$_{1-x}$)$_2$O$_3$, offering insights into the driving forces for polymorph formation that should prove useful for improved control over phase-pure growth of these important alloys.

I. INTRODUCTION

As a promising materials platform in power electronics, monoclinic Ga$_2$O$_3$ (β-Ga$_2$O$_3$) has been well characterized and studied in detail [1,2]. β-Ga$_2$O$_3$ has a band gap of 4.76–5.10 eV [3–6] and a high breakdown field of 6–8 MV/cm [7]. The existence of high-quality yet low-cost substrates [8–10] together with the ease of n-type doping [11,12] render β-Ga$_2$O$_3$ highly promising for applications in high-power electronics and UV optoelectronics [13–15].

Several polymorphs of Ga$_2$O$_3$ are known: In addition to β (monoclinic), α (corundum), γ (defective spinel), κ (orthorhombic), δ (bixbyite), and ϵ phases have been reported [16,17]. Among these polymorphs, β-Ga$_2$O$_3$ is thermodynamically the most stable and can be directly obtained from melt [8–10]. While the structures of β-, α-, γ-, and κ-Ga$_2$O$_3$ have been unambiguously identified [17–22], the space groups of the ϵ and δ polymorphs have been controversial. ϵ-Ga$_2$O$_3$ was originally assigned to a hexagonal $P6_3mc$ space group, with Ga atoms randomly occupying the octahedral and tetrahedral cation sites, yielding a disordered structure with 2:3 stoichiometry [23,24]. However, more recent high-resolution transmission electron microscopy studies [25] demonstrated that ϵ-Ga$_2$O$_3$ is composed of domains of the orthorhombic crystal structure with the space group $Pna2_1$ (i.e., the κ phase). Three connected 120° domains of the orthorhombic structure produce a pseudohexagonal symmetry, causing

ϵ-Ga$_2$O$_3$ to have been erroneously ascribed to a hexagonal symmetry. The orthorhombic Bravais lattice of ϵ-Ga$_2$O$_3$ was subsequently confirmed by high-resolution x-ray diffraction and Raman spectropy [26]. Similarly, the δ phase, first reported by Roy *et al.* [16], was subsequently suggested by Playford *et al.* to be a mixture of ϵ and β phases [27]. Therefore, there is no need to further discuss the ϵ and δ phases, and we can concentrate solely on the single phases (α, β, γ, and κ) in the present study.

It has been proposed that polymorphs of Ga$_2$O$_3$ other than β could potentially lead to advancements in gallium-oxide-based power electronics or other novel applications [28]. For example, α-Ga$_2$O$_3$ has a band gap of 5.3 eV [29,30] and has been grown epitaxially on sapphire [31]. κ-Ga$_2$O$_3$ has a band gap of 4.6–4.7 eV [28,32,33] and, uniquely among the polymorphs, has a polar structure [23,25,26] with a predicted spontaneous polarization of 23.0–26.4 μC/cm^2 [34–36]. Analogous to AlN/GaN-based heterojunctions, this polarization could be used to create an interfacial two-dimensional electron gas (2DEG) [35–37] that could be exploited in high-electron mobility transistors. In order to take advantage of these attractive features of different polymorphs of Ga$_2$O$_3$, it is crucial to understand their phase stability and unique physical properties.

Alloying with alumina further widens the band gap of β-Ga$_2$O$_3$ [38], enabling heterostructures [39–41] and the fabrication of field-effect transistors with a high-mobility two-dimensional electron gas [39]. Electron confinement depends on the conduction-band offset (CBO) between (Al$_x$Ga$_{1-x}$)$_2$O$_3$ and Ga$_2$O$_3$ [38,42–44]. The CBO increases

with Al concentration, and hence the synthesis of high-Al-fraction β-$(Al_xGa_{1-x})_2O_3$ films on top of Ga_2O_3 is desirable. This has turned out to be challenging due to formation of extended defects [45,46] and phase segregation (particularly γ phase) [47–50]. Alloying with Al has also been reported for the corundum phase, yielding a band gap that is continuously tunable from 5.4 to 8.6 eV in α-$(Al_xGa_{1-x})_2O_3$ films [31] over the entire composition range, while maintaining a high crystalline quality. A thorough understanding of the stability of the competing phases in $(Al_xGa_{1-x})_2O_3$ is needed to offer insight into how to promote formation of the desired phase while avoiding detrimental phases.

Some previous computational studies have partially addressed the issue of phase stability. Peelaers *et al.* [38] explored the relative stability of monoclinic and corundum $(Al_xGa_{1-x})_2O_3$, and Seacat *et al.* [51] investigated orthorhombic $(Al_xGa_{1-x})_2O_3$, all at zero temperature. Yoshioka *et al.* [52] did take vibrational free energies into account and investigated the phase stability of κ-, β-, and α-Ga_2O_3 up to 1500 K, but not for γ-Ga_2O_3 and $(Al_xGa_{1-x})_2O_3$ polymorphs. Our present study, based on density functional theory, addresses the phase stability of all polymorphs (α, β, γ, and κ) for both Ga_2O_3 and $(Al_xGa_{1-x})_2O_3$ alloys at both zero temperature and finite temperature.

We calculate the enthalpy of formation of different polymorphs of $(Al_xGa_{1-x})_2O_3$ and find that the γ phase is the least favorable over the entire range of Al compositions, but it exhibits a comparable enthalpy of formation to other phases around $x = 62.5\%$.

Since growth of thin alloy films often occurs pseudomorphically on Ga_2O_3 substrates, we also investigated the impact of strain on the enthalpy of formation. It was suggested that the strain would lead to the competition between β and γ phase during thin-film growth of $(Al_xGa_{1-x})_2O_3$ at high Al compositions, promoting phase segregation [47]. Specifically, we focus on the strain effect when growing β-$(Al_xGa_{1-x})_2O_3$ on top of (010)-oriented β-Ga_2O_3 substrates. Our study of the impact of strain on stability shows that the strain due to lattice mismatch between Ga_2O_3 substrates and $(Al_xGa_{1-x})_2O_3$ films only slightly increases the energy of β-$(Al_xGa_{1-x})_2O_3$ alloys due to a small increase in the enthalpy of mixing ΔH. For phases other than monoclinic, we expect ΔH to also increase with strain. The strain is highly unlikely to impact the relative phase stability since the increase in ΔH for the monoclinic phase is small.

We also performed extensive investigations of finite-temperature free energies, taking both vibrational and configurational entropy into account. For the vibrational entropy, we calculated the phonon densities of states for the various phases of Ga_2O_3, $AlGaO_3$, and Al_2O_3 at different volumes; the effect of thermal expansion at finite temperature was assessed using the quasiharmonic approximation. Referenced to the monoclinic phase of Ga_2O_3 and $AlGaO_3$, the vibrational entropy tends to stabilize the κ phase, and weakly destabilizes the α and γ phases. In Al_2O_3, the α phase remains most stable up to 1400 K, beyond which the β phase is favored due to vibrational entropy.

As for configurational entropy, the regular-solution mixing entropy gives a similar contribution for all phases at a given Al fraction and hence does not affect the relative stability of

different alloy phases. However, an additional type of configurational entropy occurs in the γ phase: This is a defective spinel phase, in which vacancies can occur in various different positions; we find that the configurational entropy associated with this disorder stabilizes the γ phase relative to the other phases.

The paper is organized as follows. In Sec. II the details of the first-principles calculations for the enthalpy of formation and free energy are introduced. The main results are presented in Sec. III. The enthalpy of formation for different polymorphs of $(Al_xGa_{1-x})_2O_3$ at zero temperature is examined in Sec. III A. Strain effect on the enthalpy of formation of $(Al_xGa_{1-x})_2O_3$ and relative phase stability is explored in Sec. III B. The vibrational and thermal properties, and the phase stability of various polymorphs of Ga_2O_3, $AlGaO_3$, and Al_2O_3 at finite temperature are investigated in Sec. III C. Since the bulk modulus characterizes elastic properties, we explore the temperature-dependent bulk modulus of various polymorphs of Ga_2O_3, $AlGaO_3$, and Al_2O_3 in Sec. III D, based on the study of thermal properties. Section IV concludes the paper.

II. METHODOLOGY

A. Structures of polymorphs

We focus on the monoclinic (β), corundum (α), orthorhombic (κ), and defective spinel (γ) phases of Ga_2O_3, Al_2O_3, and $(Al_xGa_{1-x})_2O_3$. The unit cells of these polymorphs of Ga_2O_3 are illustrated in Fig. 1. While α-Ga_2O_3 only contains octahedral cation sites, β-, κ-, γ-Ga_2O_3 contain both octahedral and tetrahedral cation sites. In the β phase, there are equal numbers of octahedral and tetrahedral sites; in the κ phase, the ratio of the octahedral and tetrahedral sites is 3:1. For the γ phase, the ratio of octahedral to tetrahedral sites depends on which cations are removed in the defective spinel phase.

Uniquely among the polymorphs, the γ-Ga_2O_3 exhibits disorder due to the fact that cation vacancies can occupy different sites within this defective spinel phase. To construct a unit cell of the γ-Ga_2O_3, we followed the two-step procedure outlined by Gutierrez *et al.* [54]: (1) Starting from the perfect conventional spinel cell $Ga_{24}O_{32}$ (corresponding to stoichiometry Ga_3O_4), create a triclinic unit cell $Ga_{18}O_{24}$ by performing a lattice transformation based on the lattice vectors $(\mathbf{a}_0, \mathbf{b}_0, \mathbf{c}_0)$ of the conventional cell:

$$\begin{pmatrix} \mathbf{a}' \\ \mathbf{b}' \\ \mathbf{c}' \end{pmatrix} = \begin{pmatrix} 0.5 & 0.5 & 0 \\ 0 & 0.5 & 0.5 \\ 1.5 & 0 & 1.5 \end{pmatrix} \begin{pmatrix} \mathbf{a}_0 \\ \mathbf{b}_0 \\ \mathbf{c}_0 \end{pmatrix}.$$

(2) Remove two Ga atoms from this triclinic unit cell to reach the desired 2:3 stoichiometry ($Ga_{16}O_{24}$). Similar to Yoshioka *et al.* [52], we removed two octahedral Ga sites which are separated by 7.9 Å, which is most energetically favorable. This results in a 5:3 ratio of octahedral to tetrahedral sites in this unit cell.

To investigate enthalpy of formation of $(Al_xGa_{1-x})_2O_3$ alloys (see Sec. III A), the alloy structures for different polymorphs can be constructed within the cells that are depicted in Figs. 1(a)–1(d), by substituting Ga with Al atoms. At a given
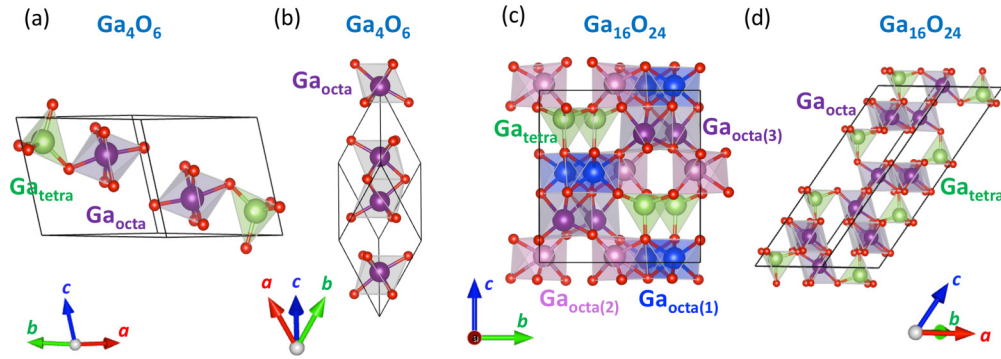
FIG. 1. Structural illustration of Ga_2O_3 polymorphs: (a) monoclinic (β); (b) corundum (α); (c) orthorhombic (κ); (d) defective spinel (γ). Red spheres denote O atoms and Ga atoms are denoted using different colors to distinguish the coordination number (see the labeling for Ga atoms). Only unit cells (a) and (b) are primitive cells. The unit cell of the defective spinel structure contains layers composed of pure tetrahedral Ga or pure octahedral Ga sites. Structural visualization was performed using VESTA [53].

Al concentration, different structures may be generated depending on which cation sites are replaced by Al. To study the thermal properties, we limited ourselves to the 50/50 $AlGaO_3$ alloy (see Sec. III C), and selected the most stable ordered $AlGaO_3$ cell for each phase as a representative example.

B. Computational details

We performed density functional calculations using the projector augmented wave method (PAW) [55] implemented in the Vienna *ab initio* simulation package (VASP) [56,57]. For all the calculations, a plane-wave energy cutoff of 500 eV was employed and the valence-electron configurations are $3d^{10}4s^24p^1$ for Ga, $3s^23p^1$ for Al, and $2s^22p^4$ for O. Note that the inclusion of Ga-$3d$ electrons in the valence is essential in the present study to obtain the correct phase ordering in Ga_2O_3 and the correct octahedral site preference of Al atoms in $(Al_xGa_{1-x})_2O_3$ [38,58]. To accurately describe the electronic structure as well as energetics, we used the hybrid functional of Heyd, Scuseria, and Ernzerhof (HSE) [59], with a mixing parameter of $\alpha = 0.32$. This results in a band gap of 4.8 eV for monoclinic Ga_2O_3 and 7.4 eV for monoclinic Al_2O_3, consistent with experiment [4,60]. Brillouin-zone integrations were carried out using a Γ-centered $4 \times 4 \times 4$ k-point mesh for the primitive cell of the monoclinic and corundum phases [Figs. 1(a) and 1(b)], a $3 \times 2 \times 2$ mesh for the orthorhombic phase [Fig. 1(c)], and a $3 \times 3 \times 1$ mesh for the defective spinel phase [Fig. 1(d) for the triclinic unit cell. Full relaxations were performed with Hellmann-Feynman forces converged to 5 meV/Å. The convergence of the structural parameters as a function of the k-point mesh was checked. The HSE-optimized structural parameters of all polymorphs of Ga_2O_3, $AlGaO_3$, and Al_2O_3 are summarized in Table I; they compare well with experiment (where available).

Calculations of interatomic force constants were performed using the generalized gradient approximation of Perdew, Burke, and Ernzerhof (PBE) for the exchange correlation [61], which is more computationally efficient and has been shown to be adequate for obtaining accurate vibrational properties [62]. The finite displacement method was used to compute the interatomic force constants, in which the forces are calculated by explicitly introducing atomic displacements

in supercells of different polymorphs. Based on the unit cells shown in Fig. 1, the supercells employed for interatomic force constant calculations are $2 \times 2 \times 2$, $2 \times 2 \times 2$, $2 \times 1 \times 1$, $2 \times 2 \times 1$ for α, β, κ, and γ phases, respectively.

C. Enthalpy of formation

The stability of alloys at zero temperature is assessed by comparing their enthalpies of formation (ΔH) with respect to the energies of the most stable structures of the end compounds, i.e., monoclinic for Ga_2O_3 and corundum

TABLE I. Structural parameters [lattice parameters (Å); angle β (degrees)] for different polymorphs of Ga_2O_3, $AlGaO_3$, and Al_2O_3, calculated using HSE. Note that the calculated lattice parameter for the defective spinel phase is a pseudocubic parameter. Available experimental lattice parameters are also listed for comparison.

	Ga_2O_3		$AlGaO_3$		Al_2O_3	
Monoclinic	Calc.	Expt.	Calc.	Expt.	Calc.	Expt.
a	12.20	12.21[a]	11.97	12.00[a]	11.76	11.85[b]
b	3.03	3.04[a]	2.95	2.98[a]	2.90	2.90[b]
c	5.79	5.81[a]	5.70	5.73[a]	5.60	5.62[b]
β	103.80	103.87[a]	104.33	104.03[a]	104.09	103.83[b]
Corundum						
a	4.96	4.98[c]	4.85	–	4.74	4.76[d]
c	13.41	13.43[c]	13.21	–	12.94	12.99[d]
Orthorhombic						
a	5.02	5.05[e]	4.91	–	4.81	4.84[f]
b	8.65	8.70[e]	8.43	–	8.31	8.33[f]
c	9.27	9.28[e]	9.11	–	8.89	8.94[f]
Spinel						
a	8.52	8.24[g]	8.33	—	8.17	7.91[b]

[a]Reference [63].
[b]Reference [64].
[c]Reference [20].
[d]Reference [65].
[e]Reference [25].
[f]Reference [66].
[g]Reference [67].

for Al_2O_3:

$$\Delta H[(Al_xGa_{1-x})_2O_3] = E[(Al_xGa_{1-x})_2O_3]$$
$$- (1-x)E[Ga_2O_3] - xE[Al_2O_3]. \quad (1)$$

These values can be fit to an expression for the enthalpy of mixing of heterostructural alloys within a regular solution model [38]:

$$\Delta H(x) = x(1-x)\Omega_0 + \Omega_1(x^2 - x)(x - 0.5)$$
$$+ (1-x)H_0 + xH_1, \quad (2)$$

where Ω_0 is the regular alloy interaction parameter, Ω_1 describes the asymmetry of the enthalpy of mixing, and H_0 and H_1 are the enthalpies of the end compounds. We have checked the convergence of the enthalpy of formation with respect to the plane-wave cutoff energy; increasing this cutoff energy from 500 to 600 eV changes the values of the enthalpy of formation by less than 5 meV per formula unit (f.u.). We note that to obtain the most accurate enthalpy of formation at zero temperature we conducted HSE calculations, while for finite-temperature properties that require phonon calculations (see Sec. II D), PBE was employed since HSE would be computationally prohibitive.

D. Free energy

To assess the relative phase stability of different polymorphs at finite temperature and constant external pressure p we use the Gibbs free energy:

$$G(p,T) = \min_V \{E(V, 0\,K) - TS^{conf}(T)$$
$$+ F^{vib}(V,T) + pV\}, \quad (3)$$

where $\min_V$ indicates the minimization of the expression value in the brackets as a function of volume V. $E(V, 0\,K)$ is the total energy of the structure at the volume V at 0 K, and S^{conf} is the configurational entropy, which can be written as $-k_B\ln\Omega$; Ω counts the number of configurations for thermodynamically equivalent macroscopic states, and k_B is the Boltzmann constant. $F^{vib}(V,T)$ is the vibrational free energy, defined as

$$F^{vib}(V,T) = \int_0^\infty d\omega g(\omega)\left[\frac{\hbar\omega}{2} + k_BT\ln(1 - e^{-\hbar\omega/k_BT})\right], \quad (4)$$

where $g(\omega)$ is the phonon density of states (DOS) at frequency ω. The interatomic force constants at a particular volume are calculated using density functional perturbation theory, as implemented in VASP. The PHONOPY code [68] is then utilized to calculate the phonon DOS and thermal properties.

The effect of thermal expansion is included using the quasiharmonic approximation (QHA), which requires both phonon calculations and total energy calculations at various fixed volumes (V). The Gibbs free energy at a given temperature and constant pressure is obtained by minimizing the free energy with respect to the volume [see Eq. (3)], resulting in the equilibrium volume at this particular temperature. Therefore, the evolution of the phonon dispersion relationship as a function of temperature is obtained by linking the temperature to the volume. We note that external pressure is zero
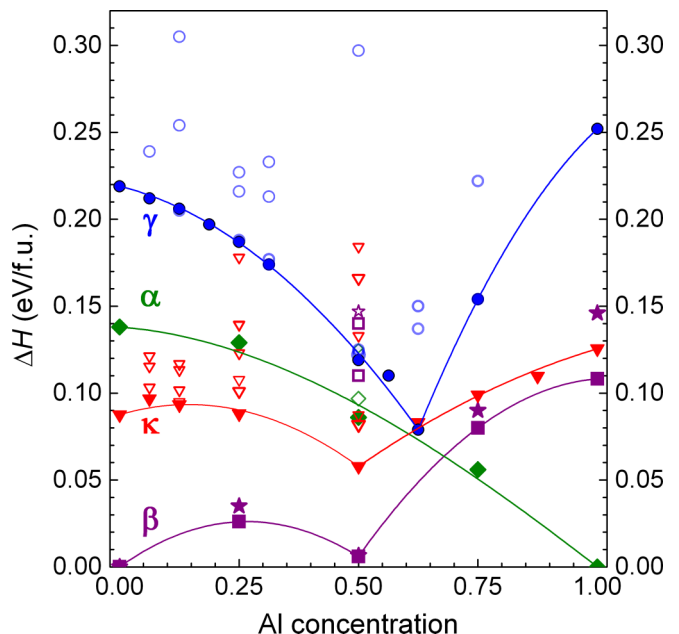

FIG. 2. Enthalpy of formation (ΔH, eV/f.u.) as a function of Al concentration for various polymorphs. The lowest energy structures are indicated by filled symbols and the higher-energy structures by open or transparent symbols. The purple stars denote the enthalpy of formation of β phase for strained (010)-oriented pseudomorphic $(Al_xGa_{1-x})_2O_3$ lattice-matched to β-Ga_2O_3. For simplicity, we use the notation β to denote the monoclinic phase across all compositions of $(Al_xGa_{1-x})_2O_3$ alloys.

throughout our calculations and therefore $pV = 0$, making the calculated Gibbs free energies only temperature dependent. From the temperature-dependent Gibbs energies, the bulk modulus as a function of temperature for different polymorphs can be obtained from Birch-Murnaghan equation-of-state fits [69,70]. In order to render the calculations affordable, the PBE exchange correlation function is employed for the study of vibrational properties, Gibbs free energy, and bulk modulus.

III. RESULTS AND DISCUSSIONS

A. Phase stability of polymorphs at 0 K

The phase stability of different polymorphs of $(Al_xGa_{1-x})_2O_3$ alloys at zero temperature is examined by comparing their enthalpies of formation ΔH [Eq. (1)]. Figure 2 shows ΔH as a function of Al concentration for β, α, κ, and γ phases. Our results for Ga_2O_3 quantitatively agree with previous calculations [38,51,52]; the relative phase stability follows the trend, in order of increasing ΔH, $\beta < \kappa < \alpha < \gamma$. The γ phase is the least stable, with a ΔH of 0.22 eV/f.u., much higher than the κ phase ($\Delta H = 0.09$ eV/f.u.) and the α phase ($\Delta H = 0.14$ eV/f.u.) (all referenced to the β phase). For the other end compound Al_2O_3, ΔH of different polymorphs follows the trend $\alpha < \beta < \kappa < \gamma$. [Note that the monoclinic phase of Al_2O_3 is conventionally denoted θ, but in order to keep a consistent notation across all compositions of $(Al_xGa_{1-x})_2O_3$ alloys we use the label β here, as for Ga_2O_3.] The γ phase is still the

TABLE II. Parameters (Ω_0, Ω_1, in units of eV) in the enthalpy of mixing of $(Al_xGa_{1-x})_2O_3$ alloys in a regular solution model [Eq. (2)]. The two values of Ω_0 for the β, κ, and γ phases result from separate piecewise fits, as explained in the text. Results from previous calculations [38] are included for comparison.

	Ω_0		Ω_1	
β	0.092 (0.081[a])	0.092 (0.101[a])	–	–
κ	0.070	0.027	–	–
α	0.096 (0.164[a])		0.043 (0.012[a])	
γ	0.098	0.078	–	–

[a]Reference [38].

least favorable ($\Delta H = 0.25$ eV/f.u.) while κ and β have similar ΔH (see Fig. 2).

As for $(Al_xGa_{1-x})_2O_3$ alloys, the relative stability between β and α phases has been explored by Peelaers *et al.* [38], and between β and κ by Seacat *et al.* [51]. Here we add the γ phase for a systematic comparison.

For α and β our calculated ΔH values agree with Ref. [38] to within $\sim$0.01 eV/f.u. Equation (2) provides a good fit for ΔH of the α phase over the entire composition range, yielding $\Omega_0 = 0.096$ eV and $\Omega_1 = 0.043$ eV compared to $\Omega_0 = 0.164$ eV and $\Omega_1 = 0.012$ eV in Ref. [38] (see Table II). For the monoclinic (β) phase, the fitting of ΔH to Eq. (2) needs to be performed in a piecewise fashion [38], due to the fact that Al prefers octahedral sites over tetrahedral sites. Equation (2) works over the entire alloy concentration range for a random solid solution, but breaks down when an alloying element exhibits a site preference. Equation (2) does hold within the individual intervals 0–0.5 and 0.5–1 within which a random solid solution model is valid. A fit of ΔH, neglecting asymmetry, yields $\Omega_0 = 0.092$ eV within both of these intervals, consistent with 0.081 and 0.101 eV in Ref. [38] (see Table II).

For the γ phase, a preference by Al atoms for the octahedral site is also observed. For low Al concentrations, different structures can be generated with Al occupying distinct octahedral sites; the resulting ΔH values are all very close to each other and barely distinguishable in Fig. 2. When Al occupies tetrahedral sites, on the other hand, ΔH is greatly increased (transparent symbols in Fig. 2). ΔH of the γ phase drops quickly when the Al concentration increases, becoming more comparable to (but still greater than) ΔH of other phases. This trend continues up to 62.5% Al, where a minimum in ΔH occurs due to all octahedral sites being occupied by Al. Beyond 62.5% Al, Al is forced to occupy tetrahedral sites, and ΔH rapidly increases to 0.25 eV/f.u. for Al_2O_3. We again fit the ΔH of the γ phase separately over the intervals 0–0.625 and 0.625–1, resulting in Ω_0 values of 0.098 and 0.078 eV for the two composition regimes.

It is worth noting that around 62.5% Al, the ΔH values of the γ, α, and κ phases are close to each other, and also closer to ΔH of β than at any lower Al content.

The κ phase contains three types of symmetry-inequivalent octahedral sites (denoted as $Ga_{octa(1)}$, $Ga_{octa(2)}$, $Ga_{octa(3)}$) and one type of tetrahedral site (Ga_{tetra}), as labeled in Fig. 1(c). We note that $Ga_{octa(3)}$ was denoted to have a pentahedral coordination in Ref. [51]; in the present study, any Ga-O pair with

a bond length less than 2.4 Å is counted as a bond, yielding three types of octahedral Ga sites. The calculated longest Ga-O bonds within the $Ga_{tetra(1)}$, $Ga_{tetra(2)}$, and $Ga_{tetra(3)}$ cation-centered octahedra are 2.03, 2.29, and 2.39 Å, respectively.

As seen from Fig. 2, the κ phase is the second most stable phase for Al concentrations up to 60.5%. The dependence of its ΔH on Al concentration is weaker than for other phases. The calculated enthalpies of formation agree with Seacat *et al.* [51]. A minimum of ΔH (0.06 eV/f.u.) is observed at 50% Al, which seems to disagree with the preference of Al for octahedral cation sites and the fact that 75% of the cation sites in the κ phase are octahedral sites. This seemingly anomalous behavior can be explained as follows: Al favors occupation of the $Ga_{octa(1)}$ and $Ga_{octa(2)}$ sites, while Al occupation of the $Ga_{octa(3)}$ (and Ga_{tetra}) sites yields a larger ΔH. This is evident from calculations at $x = 0.25$, where Al can fully occupy a single type of symmetry-inequivalent cation site; we obtained $\Delta H = 0.09$ eV/f.u. for Al on $Ga_{octa(1)}$, 0.11 eV/f.u. for $Ga_{octa(2)}$, 0.14 eV/f.u. for $Ga_{octa(3)}$, and 0.18 eV/f.u. for Ga_{tetra}. The preference for the $Ga_{octa(1)}$ and $Ga_{octa(2)}$ sites explains the dip in ΔH at $x = 0.5$. Similar to the monoclinic phase, we fit the ΔH of κ phase over the intervals 0–0.625 and 0.625–1, resulting in Ω_0 values of 0.070 and 0.027 eV for the two composition regimes.

B. Impact of strain on phase stability

Strain was suggested as an explanation for the stabilization of the γ phase, relative to β, during $(Al_xGa_{1-x})_2O_3$ thin-film growth [47]. To assess the impact of strain on phase stability, we perform a representative case study, corresponding to pseudomorphic growth of β-$(Al_xGa_{1-x})_2O_3$ lattice matched to β-Ga_2O_3 in the [010] orientation, which is most common for growth. We calculate ΔH of $(Al_xGa_{1-x})_2O_3$ with its in-plane lattice parameters constrained to those of β-Ga_2O_3, and the out-of-plane lattice parameter of $(Al_xGa_{1-x})_2O_3$ relaxed. The same structure was previously used to explore impact of strain on the band alignment [43]. Results for the strained $(Al_xGa_{1-x})_2O_3$ alloy is shown by purple stars in Fig. 1, showing only a minor impact of strain on the ΔH of $(Al_xGa_{1-x})_2O_3$, except for the end compound Al_2O_3. For Al_2O_3, the strain leads to a notable increase in ΔH, from 0.11 to 0.15 eV/f.u. The strain-induced enhancement in ΔH can be almost entirely attributed to elastic energy, which is quadratic in strain and therefore noticeably increases at larger alloy compositions due to the larger lattice mismatch and also due to the larger elastic constants of Al_2O_3 compared to Ga_2O_3.

We found that for phases other than monoclinic, ΔH similarly increases with strain. Since the ΔH increase for the monoclinic phase is small, the change in ΔH for other phases is highly unlikely to change the relative phase stability. Therefore, we do not expect strain can be the cause for phase segregation in $(Al_xGa_{1-x})_2O_3$ thin films at high Al composition, at least from a thermodynamic point of view.

C. Phase stability of polymorphs at finite temperature

In order to investigate the phase stability at finite temperatures, we considered contributions from vibrational entropy as well as configurational entropy. To calculate the Gibbs
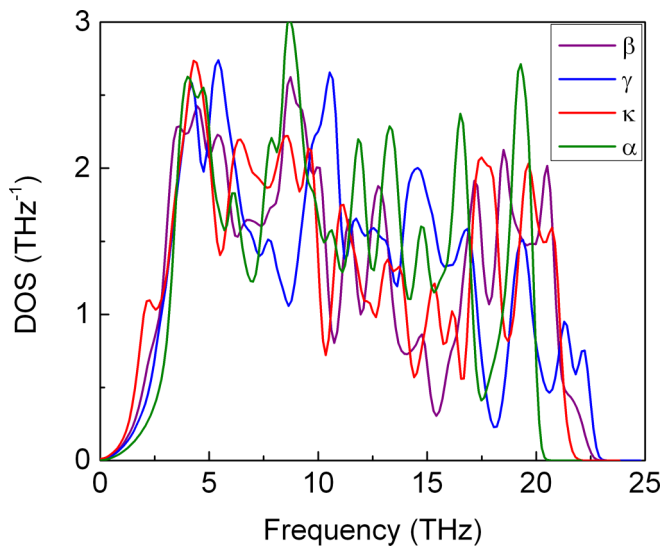
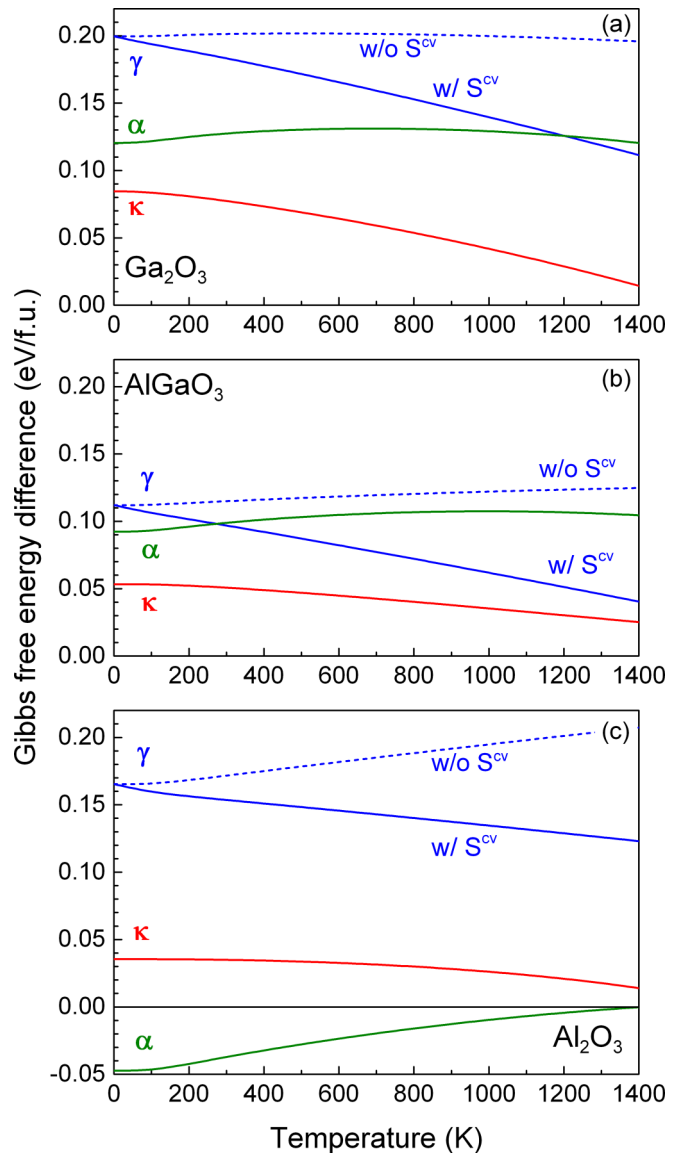FIG. 3. Phonon density of states for four polymorphs (β, α, κ, γ) of Ga_2O_3.

FIG. 4. Gibbs free-energy difference as a function of temperature for polymorphs of (a) Ga_2O_3, (b) ordered $AlGaO_3$, and (c) Al_2O_3, referenced to the monoclinic phase. Gibbs free energies of the γ phase (referenced to the monoclinic phase) with (w/) and without (w/o) S^{cv} are shown.

free energy from the phonon DOS at various crystal volumes, we employed the QHA (see Sec II D). Configurational entropy of mixing arising from random occupation of Al in $(Al_xGa_{1-x})_2O_3$ alloys (chemical disorder) is equally present in all phases since it is determined solely by the Al concentration. This type of configurational entropy will therefore not change the relative phase stability and we do include it here.

However, a different type of configurational entropy is uniquely present in the γ phase, because multiple choices are possible for removing cations from specific sites in the defective spinel structure [52]. Cation vacancy disorder is therefore inevitable in the γ phase, yielding a contribution to the configurational entropy (which we will denote as S^{cv}) that is absent in other phases, and thus could affect the relative phase stability at finite temperature.

1. Ga_2O_3

Figure 3 shows the phonon DOS of β-, α-, κ-, and γ-Ga_2O_3. One may wonder whether the choice of vacancy sites in the defective spinel structure (Sec. II A) might also affect the phonon DOS. As a check, we performed a calculation of the phonon DOS for a structure in which one octahedral and one tetrahedral Ga was removed; we found the results to be very similar to those for the most stable structure (in which the vacancies both occur on octahedral sites), leading to the conclusion that the vibrational entropy is insensitive to the details of the vacancy positions.

Low-frequency phonons play the dominant role in vibrational entropy, since they are most easily excited at finite temperatures. In the region below ~4 THz we find that the magnitude of the phonon DOS follows the trend $\alpha < \gamma < \beta < \kappa$. A peak appears in the low-frequency phonons of κ-Ga_2O_3; the atom-projected phonon DOS (not shown) indicates that this peak mainly originates from vibrations of $Ga_{octa(1)}$ and $Ga_{octa(3)}$. Due to this peak, the phonons of κ-Ga_2O_3 are more easily thermally excited than those of other phases, yielding a greater phonon population and a lowering

of the free energy relative to other phases. On the other hand, since the low-frequency phonon DOS of the α and γ phases is lower in magnitude than that of β, the α and γ phases become less stable relative to β at finite temperature.

The calculated Gibbs free energies, including the effect of lattice expansion using QHA, are plotted in Fig. 4(a). Rather than plotting absolute values, the free energies of α, κ, and γ Ga_2O_3 are referenced to the monoclinic (β) phase. The calculated Gibbs free energies of α- and κ-Ga_2O_3, referenced to that of β-Ga_2O_3, agree with Yoshioka *et al.* [52]. In line with the expectation based on the comparison of the low-frequency phonon DOS for different polymorphs, κ-Ga_2O_3 indeed becomes more stable at elevated temperatures: $F(\kappa)$-$F(\beta)$ is reduced from 0.08 to 0.02 eV/f.u. when the temperature is raised from 0 to 1400 K. This indicates that κ phase is more

likely to form thermodynamically at elevated temperature. In contrast, $F(\gamma)$-$F(\beta)$ is relatively constant with temperature, and $F(\alpha)$-$F(\beta)$ slightly increases with temperature.

To address the effect of configurational entropy associated with vacancy disorder (S^{cv}) that is uniquely present in the γ phase, we calculate the ideal configurational entropy per cation using

$$S^{cv} = k_B[c\ln(c) + (1-c)\ln(1-c)], \qquad (5)$$

where c is the concentration of cation vacancies expressed with respect to a perfect spinel structure. To achieve the stoichiometry of Ga$_2$O$_3$, c must be equal to 1/9. Here we assume that the vacancies can form on any cation sites, without taking into account that these sites have slightly different energies. This assumption overestimates S^{cv} and thus exaggerates the impact of cation vacancy disorder on the free energy. The inclusion of S^{cv} facilitates the stabilization of γ-phase Ga$_2$O$_3$ at high temperature [see Fig. 4(a)]: At 1200 K, the free energy of the γ-Ga$_2$O$_3$ is reduced to roughly the same values as for α-Ga$_2$O$_3$. However, the free-energy difference between the γ phase and the β phase is still large at these high temperatures, indicating that, thermodynamically, γ-Ga$_2$O$_3$ is still unlikely to form.

We note that stabilization of particular structures due to configurational entropy has been described in other systems. It was demonstrated that configurational entropy facilitates the formation of vacancies at high temperature in high entropy alloys [71] and in an AlB$_2$ crystal [72].

2. AlGaO$_3$

As we saw in Fig. 2, the enthalpy of formation of different polymorphs become comparable and relatively low as the Al concentration increases in (Al$_x$Ga$_{1-x}$)$_2$O$_3$ alloys, rendering it important to assess the impact of vibrational and configurational entropy on the free energy. For the ordered AlGaO$_3$ alloy with 50% Al, Fig. 4(b) shows that $F(\kappa)$-$F(\beta)$ slightly decreases with temperature while $F(\alpha)$-$F(\beta)$ slightly increases. When configurational entropy is included, $F(\gamma)$-$F(\beta)$ decreases markedly with temperature: $F(\gamma)$-$F(\beta)$ reduces from 0.11 eV/f.u. at 0 K to 0.04 eV/f.u. at 1400 K, and the γ phase becomes more stable than the α phase above 280 K.

Carrying out the free-energy calculations as displayed in Fig. 4 for additional alloy compositions would be hugely computationally expensive, due to the need for phonon calculations at different volumes within the quasiharmonic approximation, and the large supercells needed to describe lower-symmetry structures. However, the trends displayed in Fig. 4 allow drawing informative conclusions. For instance, we can examine the case of the 62.5% alloy, where according to Fig. 2 the $T = 0$ enthalpies of formation of the γ, κ, and α phases are nearly equal. From Fig. 4 we learn that the trend with temperature of the free-energy difference (referenced to the β phase) of the different polymorphs is fairly independent of the alloy composition: for the γ phase (w/S^{cv}) the free-energy difference decreases with T, for the κ phase it slightly decreases with T, and for the α phase it increases with T. It is therefore an acceptable approximation to assume that the temperature dependence of the free-energy difference will

behave similarly in the 62.5% alloys as it does in the 50% alloy. We can then take the curves from Fig. 4(b) and shift them so that the data points at $T = 0$ coincide, to reflect the fact that in the 62.5% alloy the γ, κ, and α phases have similar $T = 0$ enthalpies; the result shows that in the 62.5% alloy the γ phase is preferred over the α and κ phases at all finite temperatures.

This reduced free energy of the γ phase indicates it can form more easily in the AlGaO$_3$ alloy. Indeed, the formation of the γ phase during growth of (Al$_x$Ga$_{1-x}$)$_2$O$_3$ on β-Ga$_2$O$_3$ substrates has been reported. Bhuiyan *et al.* [47] performed metal-organic chemical vapor deposition, yielding β phase (Al$_x$Ga$_{1-x}$)$_2$O$_3$ for $x < 27\%$ but a mixed $\beta + \gamma$ phase for $27\% < x < 40\%$. Above 40% the structure became pure γ. Chang *et al.* [49] also found γ phase inclusions in (Al$_x$Ga$_{1-x}$)$_2$O$_3$ layers grown by plasma-assisted molecular beam epitaxy, but at a lower onset of Al concentration ($x < 20\%$). While the general trend that the γ phase becomes more favorable at higher Al content is in agreement with our calculations, it is also clear that the experimental results cannot be explained purely based on thermodynamics: Our results in Fig. 4 indicate the formation of the κ phase should also be expected, and do not show that single-phase γ would become more stable at the alloy compositions studied in Ref. [47]. Clearly kinetic factors associated with the growth conditions are playing an important role in actual film growth.

3. Al$_2$O$_3$

The trends in the free-energy difference as a function of temperature identified above persist in Al$_2$O$_3$. The corundum phase (α-Al$_2$O$_3$) is most stable up to $T = 1400$ K [see Fig. 4(c)]. The vibrational entropy reduces the free-energy difference between the corundum phase and the monoclinic phase of Al$_2$O$_3$, tending to destabilize the corundum phase at high T. As for the orthorhombic κ phase, it is less stable than the monoclinic phase and the free-energy difference between the two phases only slightly reduces at elevated temperature. The free energy of the γ phase is much higher than that of other phases, indicating it is less likely to form thermodynamically for Al$_2$O$_3$.

D. Bulk modulus

Figure 5 shows our results for the temperature dependence of the bulk modulus (B) for the four phases of Ga$_2$O$_3$, ordered AlGaO$_3$, and Al$_2$O$_3$, taking into account the lattice expansion at finite temperature. For Ga$_2$O$_3$, our results are in quantitative agreement with those of Yoshioka *et al.* [52] for the α, β, and κ phases. The magnitude of the bulk modulus decreases in the order $\alpha > \kappa > \beta$; the bulk modulus of the γ phase is closest to that of the κ phase.

We note that our calculated bulk modulus is somewhat underestimated due to the use of the PBE functional. Taking β-Ga$_2$O$_3$ for example, the PBE-calculated bulk modulus is 151.3 GPa at 0 K (147.1 GPa at room temperature), while the HSE-calculated bulk modulus at 0 K is 183.3 GPa (consistent with the 174 GPa value obtained using the B3LYP functional by He *et al.* [73]). The hybrid functional value is in good agreement with the experimentally measured value of 182.6 GPa (at room temperature) [74]. The underestimation
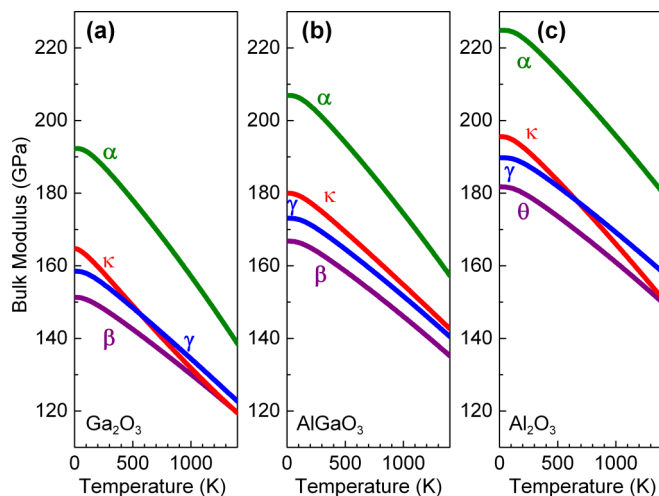
FIG. 5. Temperature dependence of the bulk modulus (B, GPa) for different polymorphs of (a) Ga_2O_3, (b) $AlGaO_3$, and (c) Al_2O_3. Here we use the commonly used notation θ to denote the monoclinic phase of Al_2O_3.

in the PBE value can be ascribed to the overestimation of the lattice parameters in PBE [58]. The underestimation of the bulk modulus using PBE is also evident for corundum Ga_2O_3: The PBE-calculated bulk modulus is 192.3 GPa at 0 K (185.6 GPa at room temperature), while the measured bulk modulus at room temperature is 221 GPa [75]. Our HSE calculation yields a value of 244 GPA (at 0 K) for α-Ga_2O_3, and B3LYP [73] gives 210 GPa. While acknowledging the underestimation associated with the PBE results, the *trends* expressed in Fig. 5 are expected to be reliable, both as a function of temperature and in terms of the relative magnitude of B for different phases. The influence of different exchange correlation functionals on the temperature dependence of the bulk modulus was studied for a series of II-VI semiconductors [76]; it was found that different functionals yield very similar trends as a function of temperature.

In addition to the temperature-dependent bulk modulus for α-, β-, and κ-Ga_2O_3, our newly calculated bulk modulus for the γ phase exhibits a similar temperature dependence as the β phase (with a slightly greater bulk modulus) and is close to the values for the κ phase [see Fig. 5(a)], with the relative ordering between γ and κ depending on temperature.

As for alloys, as shown in Fig. 5, the moduli of all polymorphs increase with Al alloying, mainly due to Al-O bonds being stronger than Ga-O bonds [58]. The overall trend roughly stays the same across the three materials, with the α phase exhibiting the largest bulk modulus over the entire studied temperature range.

We expect that the magnitude of the bulk modulus is correlated with the density ρ of the different polymorphs, since $B = \rho \frac{dP}{d\rho}$, where $\frac{dP}{d\rho}$ denotes the derivative of pressure with respect to density. We found a linear correlation between the 0 K bulk modulus and the density for the different polymorphs of Ga_2O_3 and Al_2O_3. The reason that the α phase always has a greater bulk modulus than the other phases is primarily due to its higher density.

IV. CONCLUSIONS

We have reported a comprehensive investigation of phase stability of several polymorphs of $(Al_xGa_{1-x})_2O_3$, including the monoclinic β phase, the corundum α phase, the orthorhombic κ phase, and the defective spinel γ phase. We found that, as previously observed for β-$(Al_xGa_{1-x})_2O_3$ [38], both κ- and γ-$(Al_xGa_{1-x})_2O_3$ exhibit a minimum in their enthalpy of formation as a function of Al concentration, which we attribute to Al atoms preferring to occupy the octahedral cation sites. γ-$(Al_xGa_{1-x})_2O_3$ has the highest enthalpy of formation over the entire composition range. The enthalpy of formation of γ-$(Al_xGa_{1-x})_2O_3$ exhibits the strongest dependence on Al concentration; it is lowest at 62.5% Al, where it becomes comparable to that of other phases. The enthalpy of formation of the κ phase, the second most stable phase up to 62.5% Al, varies less as a function of Al concentration.

The finite temperature phase stability of $(Al_xGa_{1-x})_2O_3$ was assessed by comparing the Gibbs free energy of different polymorphs, taking into account the vibrational entropy as well as configurational entropy; the latter is particularly relevant for the γ phase due to the presence of vacancy disorder in the defective spinel structure. Thermal expansion was included using the quasiharmonic approximation. Across the alloy range, the lattice vibrations tend to render the κ phase more stable at higher temperatures, while destabilizing the α and γ phases relative to the monoclinic phase. We attributed this to the relative magnitude of the phonon DOS in the low-frequency region. Configurational entropy arising from cation vacancy disorder in the spinel structure was found to play a key role in stabilizing the γ phase and rendering it increasingly more competitive with other phases at increasing Al concentrations.

An important conclusion from our study is that the monoclinic β phase is thermodynamically stable for $(Al_xGa_{1-x})_2O_3$ alloy concentrations up to at least 50% and temperatures up to at least 1400 K. This is consistent with experimental results on bulk crystals (see Ref. [77] and other references in Ref. [38]), but leaves unexplained why thin-film growth of $(Al_xGa_{1-x})_2O_3$ on Ga_2O_3 substrates has resulted in phase segregation [47–50] at Al concentrations well below 50%. Our present study indicates that strain does not provide an explanation. The systematic observation of the γ phase when phase segregation occurs is even more puzzling, since γ is not even the next-most-stable phase after β (see Fig. 4). Future investigations are called for to identify the kinetic factors that favor formation of the γ phase during growth of epitaxial alloy films.

[1] S. J. Pearton, J. Yang, P. H. Cary IV, F. Ren, J. Kim, M. J. Tadjer, and M. A. Mastro, Appl. Phys. Rev. **5**, 011301 (2018).

[2] M. Higashiwaki and S. Fujita, *Gallium Oxide: Materials Properties, Crystal Growth, and Devices* (Springer Nature, New York, 2020), Vol. 293.

[3] H. Tippins, Phys. Rev. **140**, A316 (1965).

[4] T. Matsumoto, M. Aoki, A. Kinoshita, and T. Aono, Jpn. J. Appl. Phys. **13**, 1578 (1974).

[5] C. Sturm, R. Schmidt-Grund, C. Kranert, J. Furthmüller, F. Bechstedt, and M. Grundmann, Phys. Rev. B **94**, 035148 (2016).

[6] A. Mock, R. Korlacki, C. Briley, V. Darakchieva, B. Monemar, Y. Kumagai, K. Goto, M. Higashiwaki, and M. Schubert, Phys. Rev. B **96**, 245205 (2017).

[7] M. Higashiwaki, K. Sasaki, A. Kuramata, T. Masui, and S. Yamakoshi, Appl. Phys. Lett. **100**, 013504 (2012).

[8] E. G. Víllora, K. Shimamura, Y. Yoshikawa, K. Aoki, and N. Ichinose, J. Cryst. Growth **270**, 420 (2004).

[9] Y. Tomm, P. Reiche, D. Klimm, and T. Fukuda, J. Cryst. Growth **220**, 510 (2000).

[10] A. Kuramata, K. Koshi, S. Watanabe, Y. Yamaoka, T. Masui, and S. Yamakoshi, Jpn. J. Appl. Phys. **55**, 1202A2 (2016).

[11] J. B. Varley, J. R. Weber, A. Janotti, and C. G. Van de Walle, Appl. Phys. Lett. **97**, 142106 (2010).

[12] J. L. Lyons, D. Steiauf, A. Janotti, and C. G. Van de Walle, Phys. Rev. Appl. **2**, 064005 (2014).

[13] R. Suzuki, S. Nakagomi, Y. Kokubun, N. Arai, and S. Ohira, Appl. Phys. Lett. **94**, 222102 (2009).

[14] T. Oshima, T. Okuno, N. Arai, N. Suzuki, S. Ohira, and S. Fujita, Appl. Phys. Express **1**, 011202 (2008).

[15] F. Alema, B. Hertog, P. Mukhopadhyay, Y. Zhang, A. Mauze, A. Osinsky, W. V. Schoenfeld, J. S. Speck, and T. Vogt, APL Mater. **7**, 022527 (2019).

[16] R. Roy, V. Hill, and E. Osborn, J. Am. Chem. Soc. **74**, 719 (1952).

[17] K. Matsuzaki, H. Yanagi, T. Kamiya, H. Hiramatsu, K. Nomura, M. Hirano, and H. Hosono, Appl. Phys. Lett. **88**, 092106 (2006).

[18] J. Kohn, G. Katz, and J. Broder, Am. Mineral. **42**, 398 (1957).

[19] J. Åhman, G. Svensson, and J. Albertsson, Acta Crystallogr. Sect. C **52**, 1336 (1996).

[20] M. Marezio and J. Remeika, J. Chem. Phys. **46**, 1862 (1967).

[21] M. Zinkevich, F. M. Morales, H. Nitsche, M. Ahrens, M. Rühle, and F. Aldinger, Int. J. Mater. Res. **95**, 756 (2004).

[22] C. O. Areán, A. L. Bellan, M. P. Mentruit, M. R. Delgado, and G. T. Palomino, Microporous Mesoporous Mater. **40**, 35 (2000).

[23] F. Mezzadri, G. Calestani, F. Boschi, D. Delmonte, M. Bosi, and R. Fornari, Inorg. Chem. **55**, 12079 (2016).

[24] F. Boschi, M. Bosi, T. Berzina, E. Buffagni, C. Ferrari, and R. Fornari, J. Cryst. Growth **443**, 25 (2016).

[25] I. Cora, F. Mezzadri, F. Boschi, M. Bosi, M. Čaplovičová, G. Calestani, I. Dódony, B. Pécz, and R. Fornari, CrystEngComm **19**, 1509 (2017).

[26] M. Kracht, A. Karg, J. Schörmann, M. Weinhold, D. Zink, F. Michel, M. Rohnke, M. Schowalter, B. Gerken, A. Rosenauer *et al.*, Phys. Rev. Appl. **8**, 054002 (2017).

[27] H. Y. Playford, A. C. Hannon, E. R. Barney, and R. I. Walton, Chem. Eur. J. **19**, 2803 (2013).

[28] J. L. Lyons, ECS J. Solid State Sci. Technol. **8**, Q3226 (2019).

[29] D. Shinohara and S. Fujita, Jpn. J. Appl. Phys. **47**, 7311 (2008).

[30] A. Segura, L. Artús, R. Cuscó, R. Goldhahn, and M. Feneberg, Phys. Rev. Mater. **1**, 024604 (2017).

[31] R. Jinno, C. S. Chang, T. Onuma, Y. Cho, S.-T. Ho, D. Rowe, M. C. Cao, K. Lee, V. Protasenko, D. G. Schlom *et al.*, Sci. Adv. **7**, eabd5891 (2021).

[32] M. Mulazzi, F. Reichmann, A. Becker, W. Klesse, P. Alippi, V. Fiorentini, A. Parisini, M. Bosi, and R. Fornari, APL Mater. **7**, 022522 (2019).

[33] M. Pavesi, F. Fabbri, F. Boschi, G. Piacentini, A. Baraldi, M. Bosi, E. Gombia, A. Parisini, and R. Fornari, Mater. Chem. Phys. **205**, 502 (2018).

[34] J. Kim, D. Tahara, Y. Miura, and B. G. Kim, Appl. Phys. Express **11**, 061101 (2018).

[35] S. B. Cho and R. Mishra, Appl. Phys. Lett. **112**, 162101 (2018).

[36] M. B. Maccioni and V. Fiorentini, Appl. Phys. Express **9**, 041102 (2016).

[37] Y. Kuang, X. Chen, T. Ma, Q. Du, Y. Zhang, J. Hao, F.-F. Ren, B. Liu, S. Zhu, S. Gu *et al.*, ACS Appl. Electron. Mater. **3**, 795 (2021).

[38] H. Peelaers, J. B. Varley, J. S. Speck, and C. G. Van de Walle, Appl. Phys. Lett. **112**, 242101 (2018); **115**, 159901 (2019) (erratum).

[39] Y. Zhang, C. Joishi, Z. Xia, M. Brenner, S. Lodha, and S. Rajan, Appl. Phys. Lett. **112**, 233503 (2018).

[40] S. Krishnamoorthy, Z. Xia, C. Joishi, Y. Zhang, J. McGlone, J. Johnson, M. Brenner, A. R. Arehart, J. Hwang, S. Lodha *et al.*, Appl. Phys. Lett. **111**, 023502 (2017).

[41] P. Ranga, A. Bhattacharyya, A. Chmielewski, S. Roy, R. Sun, M. A. Scarpulla, N. Alem, and S. Krishnamoorthy, Appl. Phys. Express **14**, 025501 (2021).

[42] A. A. U. Bhuiyan, Z. Feng, J. M. Johnson, H.-L. Huang, J. Hwang, and H. Zhao, Appl. Phys. Lett. **117**, 252105 (2020).

[43] S. Mu, H. Peelaers, Y. Zhang, M. Wang, and C. G. Van de Walle, Appl. Phys. Lett. **117**, 252104 (2020).

[44] R. Wakabayashi, M. Hattori, K. Yoshimatsu, K. Horiba, H. Kumigashira, and A. Ohtomo, Appl. Phys. Lett. **112**, 232103 (2018).

[45] A. Anhar Uddin Bhuiyan, Z. Feng, J. M. Johnson, Z. Chen, H.-L. Huang, J. Hwang, and H. Zhao, Appl. Phys. Lett. **115**, 120602 (2019).

[46] J. M. Johnson, H.-L. Huang, M. Wang, S. Mu, J. B. Varley, A. A. Uddin Bhuiyan, Z. Feng, N. K. Kalarickal, S. Rajan, H. Zhao *et al.*, APL Mater. **9**, 051103 (2021).

[47] A. A. U. Bhuiyan, Z. Feng, J. M. Johnson, H.-L. Huang, J. Sarker, M. Zhu, M. R. Karim, B. Mazumder, J. Hwang, and H. Zhao, APL Mater. **8**, 031104 (2020).

[48] J. Sarker, S. Broderick, A. A. U. Bhuiyan, Z. Feng, H. Zhao, and B. Mazumder, Appl. Phys. Lett. **116**, 152101 (2020).

[49] C. S. Chang, N. Tanen, V. Protasenko, T. J. Asel, S. Mou, H. G. Xing, D. Jena, and D. A. Muller, APL Mater. **9**, 051119 (2021).

[50] A. Hassa, C. Wouters, M. Kneiß, D. Splith, C. Sturm, H. von Wenckstern, M. Albrecht, M. Lorenz, and M. Grundmann, J. Phys. D: Appl. Phys. **53**, 485105 (2020).

[51] S. Seacat, J. L. Lyons, and H. Peelaers, Appl. Phys. Lett. **116**, 232102 (2020).

[52] S. Yoshioka, H. Hayashi, A. Kuwabara, F. Oba, K. Matsunaga, and I. Tanaka, J. Phys.: Condens. Matter **19**, 346211 (2007).

[53] K. Momma and F. Izumi, J. Appl. Crystallogr. **44**, 1272 (2011).

[54] G. Gutiérrez, A. Taga, and B. Johansson, Phys. Rev. B **65**, 012101 (2001).

[55] P. E. Blöchl, Phys. Rev. B **50**, 17953 (1994).

[56] G. Kresse and J. Hafner, Phys. Rev. B **48**, 13115 (1993).

[57] G. Kresse and J. Furthmüller, Phys. Rev. B **54**, 11169 (1996).

[58] S. Mu, H. Peelaers, and C. G. Van de Walle, Appl. Phys. Lett. **115**, 242103 (2019).

[59] J. Heyd, G. E. Scuseria, and M. Ernzerhof, J. Chem. Phys. **118**, 8207 (2003); **124**, 219906 (2006).

[60] R. Franchy, G. Schmitz, P. Gassmann, and F. Bartolucci, Appl. Phys. A **65**, 551 (1997).

[61] J. P. Perdew, K. Burke, and M. Ernzerhof, Phys. Rev. Lett. **77**, 3865 (1996).

[62] B. Grabowski, T. Hickel, and J. Neugebauer, Phys. Rev. B **76**, 024309 (2007).

[63] C. Kranert, M. Jenderka, J. Lenzner, M. Lorenz, H. Von Wenckstern, R. Schmidt-Grund, and M. Grundmann, J. Appl. Phys. **117**, 125703 (2015).

[64] R.-S. Zhou and R. L. Snyder, Acta Crystallogr. Sect. B **47**, 617 (1991).

[65] E. Newnham and Y. De Haan, Z. Kristallogr. **117**, 235 (1962).

[66] B. Ollivier, R. Retoux, P. Lacorre, D. Massiot, and G. Férey, J. Mater. Chem. **7**, 1049 (1997).

[67] H. Y. Playford, A. C. Hannon, M. G. Tucker, D. M. Dawson, S. E. Ashbrook, R. J. Kastiban, J. Sloan, and R. I. Walton, J. Phys. Chem. C **118**, 16188 (2014).

[68] A. Togo and I. Tanaka, Scr. Mater. **108**, 1 (2015).

[69] F. D. Murnaghan, Proc. Natl. Acad. Sci. USA **30**, 244 (1944).

[70] F. Birch, Phys. Rev. **71**, 809 (1947).

[71] X. Zhang, S. V. Divinski, and B. Grabowski, Acta Mater. **227**, 117677 (2022).

[72] E. Johansson, F. Eriksson, A. Ektarawong, J. Rosen, and B. Alling, J. Appl. Phys. **130**, 015110 (2021).

[73] H. He, R. Orlando, M. A. Blanco, R. Pandey, E. Amzallag, I. Baraille, and M. Rérat, Phys. Rev. B **74**, 195123 (2006).

[74] K. Adachi, H. Ogi, N. Takeuchi, N. Nakamura, H. Watanabe, T. Ito, and Y. Ozaki, J. Appl. Phys. **124**, 085102 (2018).

[75] K. E. Lipinska-Kalita, P. E. Kalita, O. A. Hemmers, and T. Hartmann, Phys. Rev. B **77**, 094123 (2008).

[76] J. M. Skelton, D. Tiana, S. C. Parker, A. Togo, I. Tanaka, and A. Walsh, J. Chem. Phys. **143**, 064710 (2015).

[77] V. Hill, R. Roy, and E. Osborn, J. Am. Ceram. Soc. **35**, 135 (1952).